A Preliminary Study of Three-Dimensional Turbulent Flow over Vortex Generators with a Plenoptic Camera

Lauren P. McManus[1]
Auburn University, Auburn, AL, 36849

For this study, the potential drag reducing nature of turbulent flow is considered. Higher energy turbulent flow better resists separation compared to laminar flow, helping to reduce induced drag. Vortex generators (VGs) can be used to either trip laminar flow to turbulent, or to promote strong streamwise vortices in already turbulent flow. To truly gain insight into the turbulent structures produced VGs, as well as interactions between the structures, a 3-D diagnostic technique must be used. The 3-D flow field of a Wheeler doublet vane vortex generator was studied using a newly emerging technique called plenoptic PIV. Plenoptic PIV measures the instantaneous 3-D velocity field of a turbulent flow using the novel light-field capturing ability of a plenoptic camera. From one setup of the plenoptic camera, a full 3-D vector field is produced, allowing 3-D flow features to be studied. Traditional 2-D PIV type data can also be gathered in any plane, at any slice in the volume. The plenoptic camera offers more data from a single run than any other diagnostics method available. Traditional PIV was also applied to measure the instantaneous 2-D velocity field at the same areas downstream from the vortex generators. Two-dimensional image slices obtained using the plenoptic camera agree with previous studies on VGs as well as the traditional 2-D PIV images obtained in this study, validating the plenoptic camera as a viable diagnostic method for studying vortex generators. The 3-D vector field obtained by the plenoptic camera also shows similar flow characteristics to those observed in previous studies with VGs. The plenoptic camera is shown to be a viable method to capture 3-D structures and their interactions in turbulent boundary layer flow.

Nomenclature

δ	=	boundary layer thickness
θ	=	momentum thickness
δ^*	=	displacement thickness
H	=	shape factor
l	=	length scale
Re	=	Reynolds number
u	=	characteristic speed
U_∞	=	freestream velocity
μ	=	viscosity of fluid
ρ	=	density of fluid

I. Introduction

Vortex generators (VGs) are devices that are used to excite a turbulent boundary layer, usually with the intent of or preventing flow separation. Vortex generators shed stream-wise vortices which supply momentum from high momentum regions of the flow to lower momentum regions. This distribution of momentum creates a higher energy boundary layer. Vortex generators are used in a variety of practical applications in engineering. Vortex generators can increase lift and/or reduce drag on various airfoils, as well as reduce aircraft interior noise[1]. VGs do increase local surface drag, but in applications on airplane wings or car roofs, they can help to decrease global drag

[1] Undergraduate Research Assistant, Department of Aerospace Engineering, 335 Aerospace Engineering Building, Auburn, AL 36849, Student Member Grade

by reducing the size of the separation wake where large amounts of induced drag are created[2]. One of the primary causes of drag on sedans is actually the separation of flow near the rear end of the vehicle, which motivated Mitsubishi's use of VGs in Reference 2. VGs can also be used in chemical engineering applications to enhance mixing in chemical reactions[3].

The vortices created by VGs are 3-D, and coherent structures such as hairpin or horseshoe vortices can also be observed. The study of the effect of VGs on turbulent flow necessitates 3-D flow diagnostics. Three-dimensional methods for studying turbulence have come into light in just the past few years. Defocusing PIV, holographic PIV, tomographic PIV, and synthetic aperture PIV are all noted for their ability to capture 3-D, 3-C flow fields, yet they are hindered by complicated optical set-ups and difficulties in the reconstruction process[4,5]. A solution to the difficulties faced with studying 3-D, 3-C flow fields is digital light field imaging. Light field imaging using a plenoptic camera is a relatively simplified means of potentially obtaining 3-D, 3-C data for a velocity field.

This paper demonstrates the ability of the plenoptic camera to study the 3-D flow effects created by vortex generators. Success of the plenoptic camera in studying passive vortex generators sets the stage for the potential of more in-depth study of passive flow control methods as well as eventually active flow control.

II. Boundary Layer Parameters

The Reynolds number is a quantity associated with a flow that takes into account the impact of the fluid viscosity (μ), the fluid density (ρ), the characteristic speed (u), and a length scale (l). The length scale is important because many different scales can be used in order to define Reynolds numbers for different flow properties. The equation for the Reynolds number is:

$$Re = \frac{\rho u l}{\mu} \tag{1}$$

One of the most common length scales associated with a boundary layer is the boundary layer thickness. The boundary layer thickness (δ) is usually defined as the distance from the wall to the point in the flow where the velocity reaches 99% of the free stream velocity. For turbulent boundary layers, the boundary layer thickness grows more rapidly than in laminar boundary layers as the flow moves downstream[6]. There are several additional properties commonly used to describe boundary layers. One property is the displacement thickness, δ^*. The displacement thickness can be interpreted as the missing mass flow due to the boundary layer. The displacement thickness is also what creates the concept of an effective body because a streamline that is outside of the boundary layer is deflected upward by a distance of δ^*. The equation for the displacement thickness for incompressible flow is[6]:

$$\delta^* = \int_0^y \left(1 - \frac{u}{U_\infty}\right) dy \tag{2}$$

Another important boundary layer property is the momentum thickness, θ. The momentum thickness is the decrease in momentum across the boundary layer thickness. The equation for the momentum thickness for incompressible flow is[6]:

$$\theta = \int_0^y \frac{u}{U_\infty}\left(1 - \frac{u}{U_\infty}\right) dy \tag{3}$$

Reynolds numbers can be calculated to characterize a flow using the boundary layer thickness, the displacement thickness, or the momentum thickness as the length scale. A final property commonly used to describe boundary layer flow is the shape factor, H. The shape factor is the ratio between the displacement thickness and the momentum thickness:

$$H = \frac{\delta^*}{\theta} \tag{4}$$

For laminar flow the shape factor is around 2.6, and for turbulent flow the shape factor is approximately 1.3[6].

III. Turbulent Flow over Vortex Generators

Turbulence is an elusive concept and one of the final physical phenomenon yet to be fully understood. A pure theory does not exist for turbulent behavior, and even the definition of turbulence can be ambiguous. An occurrence often associated with turbulent flow is the boundary layer. The boundary layer in itself also presents many unsolved problems and unknowns.

Turbulent boundary layers are often pervaded by coherent structures. These coherent structures are robust vortical structures that maintain their form over many turn-over times[7]. The most common of these structures in a boundary layer is the hairpin vortex. Hairpin vortices form from mean flow vortex tubes aligned along the z-axis (Fig. 1a). These tubes are almost "frozen" into the fluid at high Reynolds numbers. However, a stream-wise gust can sweep out an axial component of this vorticity (Fig. 1b), and the mean flow continues to stretch out this long, arch-like vorticity so that it resembles a hairpin or a horse-shoe oriented at 45˚ to the mean flow[7] (Fig. 1c and 1d). The most common view on the interaction of turbulence structures within wall-bounded flows is that the near-wall structures develop into large-scale, outer-layer structures, but not the other way around[8]. These hairpin vortices populate the outer region of the flow at low and moderate Reynolds numbers and align coherently to create larger-scale structures which are called packets or forests. These packets in the outer layer of rough-wall flow induce strong ejections of fluid away from the wall[9]. It is possible that the buffer region between the boundary layer and the outer flow may be penetrated by structures with outer-length scales such as hairpin vortices. Therefore, 3-D coherent structures may be critical in understanding how manipulations to the boundary layer, such as the addition of vortex generators, will affect the mean flow.

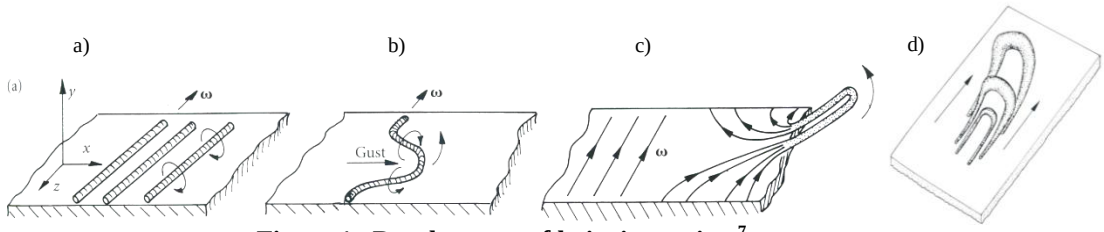

Figure 1. Development of hairpin vortices[7].

VGs are most effective when applied to flows that experience an adverse pressure gradient. An adverse pressure gradient is when flow moves from a region of low static pressure to a region with higher static pressure. This occurs as flow moves over a wing or over the roof of a car. An adverse pressure gradient tends to resist the motion of the flow, and eventually leads to flow separation as the pressure forces become strong enough. This causes induced drag in the form of pressure drag to drastically increase due to the formation of a separation wake[10]. Vortex generators were developed to create stream-wise vortices which mix the free-stream flow with the boundary layer flow in order to delay or even completely prevent flow separation[10]. A variety of vortex generators can be seen in Figure 2. A forward facing wedge (Fig. 2a), a backward-facing wedge (Fig. 2b), wishbone Wheeler vanes (Fig. 2c), and doublet Wheeler vanes (Fig. 2d) are all shown. Since VGs protrude into the flow, they do increase drag locally, but if designed correctly, they will reduce the global drag by discouraging separation[2]. The doublet Wheeler vortex generators (U.S. patent 4455045) used in this study were intended for use on the back of a car roof, just ahead of the back windshield, as this is where a large turbulent wake begins to form. However, Cessna Aircraft Company was the first customer and vortex generators of all types have been used on many aircraft wings.

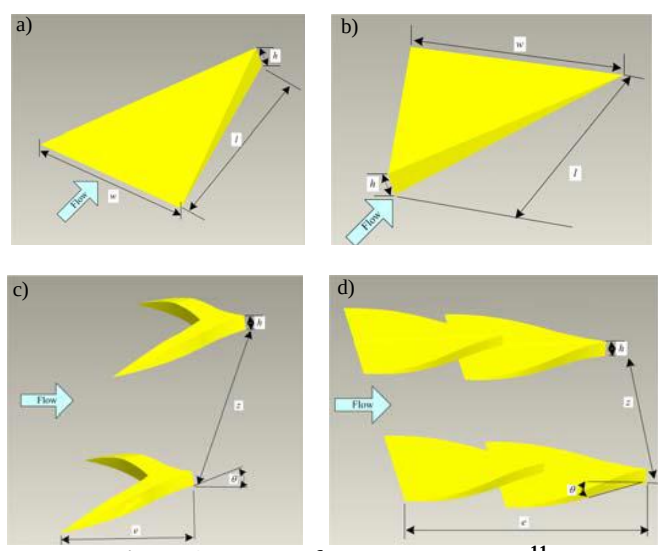

Figure 2. Types of vortex generators[11].

Vortex generators are able to energize the boundary layer flow by creating trailing, stream-wise vortices which mix with the freestream and pull the freestream flow into the boundary layer[11]. This increases the momentum near the wall by transferring momentum from the freestream flow to the wall-region[2]. The vortices created by VGs are 3-D, as are the other effects of the VGs. Barter and Dolling conducted an experiment with Wheeler doublet vortex generators and noted that the VGs produced "significant three-dimensionality", creating a fuller boundary layer with increased turbulence in the boundary layer[11]. In a study by Lu, et al. [11] of supersonic flow over Wheeler doublet VGs, a weak horseshoe vortex appeared at the leading edge of the VGs. There were also two pairs of vortices shed: a primary pair formed at the corners of the leading edge, and a secondary pair shedding off the sides before reaching the tip of the VGs. The horseshoe vortex actually acted to confine the primary vortex pair, forcing them to trail downstream and eventually intersect. These flow features can be seen in Figure 3. When the opposing vortices of either the primary or secondary pair intersected, the symmetry broke, contributing to the unsteadiness inherent in turbulence. Interestingly, no visible interference was noted in the span-wise direction between the VGs, despite their close proximity.

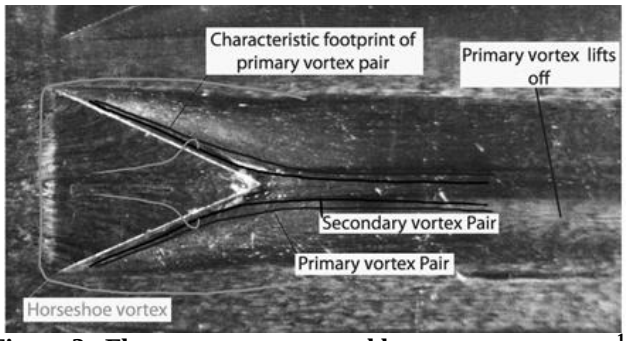

Figure 3. Flow structures created by vortex generators[11].

Vortex generators can also be used in chemical engineering applications to increase mixing in a chemical reaction. The micro-mixing characteristic size is directly related with the energy dissipation rate of turbulence[3]. Therefore, control of the dissipation rate of the turbulence allows for control of the mixing rate. Mokrani, et al. [3] used trapezoidal tabs as vortex generators. These tabs generated longitudinal vortical structures as well as enhanced turbulence, leading to a decrease in the characteristic length of micro-mixing. Even though these tabs are trapezoidal, much of the effects are likely to be the similar to the Wheeler doublet vortex generators since both are ramp-like. As fluid flows up the ramp, a small wake forms behind the ramp so that the fluid velocity at the wall behind the VG is lower than the flow over the top of the VG. This causes the pressure on the top of the VG to become lower than the pressure at the wall, forming a pair of counter-rotating vortices as seen in Figure 4. These vortices were found to increase the rate of kinetic energy flux as well as intensify friction and heat transfer[3]. The vortices have a "mushroom" cross-section with a height of the same order of the height of the tabs. Hairpin vortices also formed and rode on top of the primary longitudinal vortices. However, with respect to the application of mixing for chemical processes, the hairpin vortices were found to contribute less to the radial transport mixing than the stream-wise vortices. The non-dimensional axial velocity results found by Mokrani also indicated interesting flow behavior downstream of the VGs. Minimum values of axial velocity near the wall indicate momentum transfer as the longitudinal vortices transfer low-momentum from the wall-region to the free-stream, decreasing the magnitude of the velocity. However, further downstream as the vortices break up into more chaotic turbulent flow, the unsteady velocity fluctuations even out the momentum distributions, decreasing the drop in velocity near the wall[3].

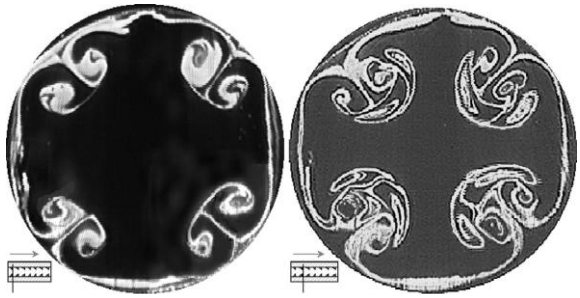

Figure 4. Counter-rotating vortices behind vortex generators[3].

All studies with VGs noted similar flow effects: hairpin and horseshoe vortices, strong longitudinal (stream-wise) vortex pairs, and increased levels of turbulence and momentum dissipation. Figure 5 shows a Schlieren image of the increased turbulence and boundary layer growth downstream of a vortex generator. These effects are strongly three-dimensional and require novel 3-D flow diagnostic techniques to be studied most effectively.

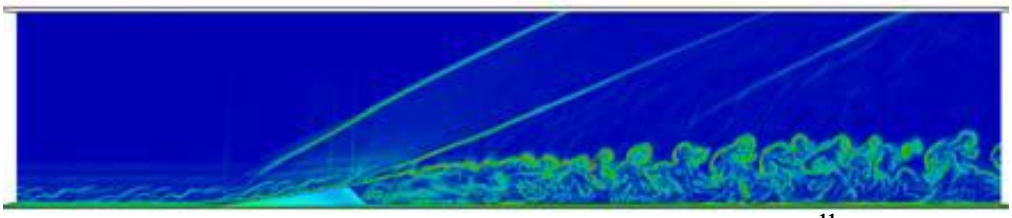

Figure 5. Schlieren image of turbulent flow behind a VG[11].

IV. Digital Light Field Photography

Traditional particle image velocimetry (PIV) is two-dimensional (2-D) and cannot fully capture the coherent structures present in turbulent flow, which are 3-D in nature. Other methods of flow visualization such as Schlieren imaging are also limited to 2-D. Stereoscopic PIV allows for three-component (3-C) measurements within a 2-D plane but the out-of-plane spatial resolution is very low compared to the in-plane resolution[4]. High speed scanning and subsequent imaging can also provide 3-D flow visualization by using bursts of high energy lasers through cylindrical lenses to create a thin laser sheet that "slices" the flow. There are also some techniques that have shown promise for collecting 3-D, 3-C data. These are defocusing PIV, holographic PIV, tomographic PIV (tomo-PIV), and synthetic aperture PIV (SAPIV). These four methods, in addition to stereoscopic PIV, are generally restricted to particle based measurements (i.e., PIV) and are not well suited for flow visualization[5]. In contrast, the scanning and imaging method described is better suited for flow visualization and not for actual particle data collection. Ultimately, a process that requires a relatively simple set-up and post-process, with the ability to perform both flow visualization and particle based measurements would be invaluable in the 3-D, 3-C study of turbulent flow. The use of digital light field photography may be the solution to this dilemma.

Digital light field photography promises to solve the persistent problem of focusing. The root of this problem is a lack of data. A camera can be enhanced by micron-scale changes to its optics and sensor so that it can sample the total geometric distribution of light. A super-representation of the lighting inside the camera allows for enormous flexibility and control when computing the final output image[12]. The process is well detailed by Ren Ng in Reference 12, but is briefly described herein.

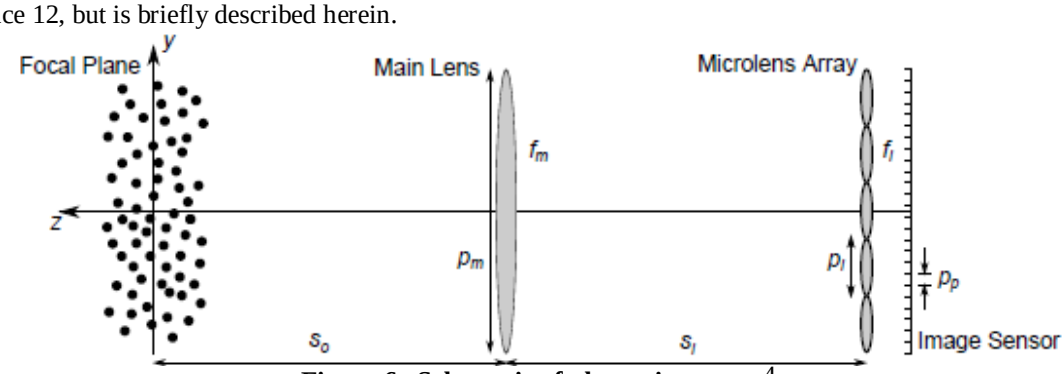

Figure 6. Schematic of plenoptic camera[4].

A plenoptic camera is a device that uses a microlens array mounted close to a CCD to encode the angular information of the incident rays of the light field onto pixels behind each microlens[4]. Figure 6 shows the elements that comprise the plenoptic camera. A microlens array in front of the image sensor records the light field inside the camera. Each microlens covers a small array of image sensor pixels. The number of pixels behind each microlens corresponds to the number of views available. The microlenses separate the light that strikes them into a tiny image, forming a mini picture of the incident lighting. This allows the light field inside the camera to be sampled in a single photographic exposure. The microlenses in a plenoptic camera simulate an eccentric aperture. An eccentric displaces an object based on its distance from the lens as shown by Figure 7. With the plenoptic camera, incoming

rays fall on different pixels behind the microlens array, indicating near and far objects, as show in Figure 8. By analyzing the distribution of the pixels accumulated, the depth of the object can be found. A refocused image can be formed by integrating the pixels that fall within a specified radius of each microlens[4]. This technique, known as ray tracing, can be used to create a refocused image at any plane using the known angular and spatial coordinates of each pixel. The series of 2-D images at many planes within the image are later "stacked" to form a complete 3-D image. The refocusing ability of digital light field technology is the key to the potential of 3-D imaging.

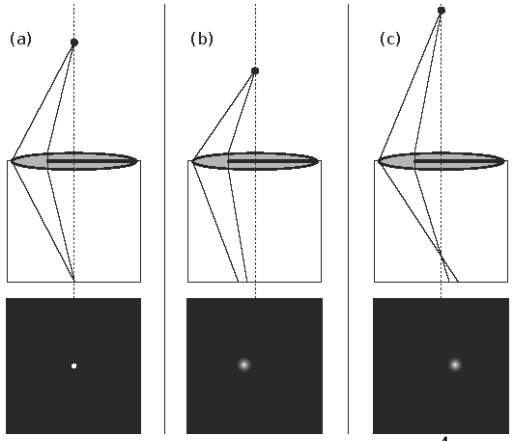

Figure 7. Eccentric aperture lens[4].

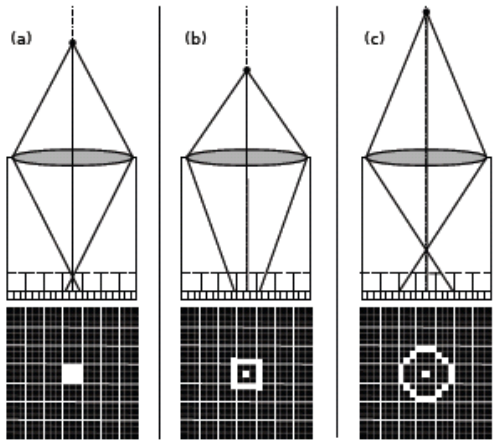

Figure 8. Pixels behind plenoptic camera microlens array[4].

V. Experimental Setup

Traditional 2-D PIV was performed as a complement to the plenoptic camera images. The images for the 2-D PIV and the plenoptic camera were taken of the same test sections to allow for comparison, as seen in Figure 9. Auburn's 0.6096 meter by 0.6096 meter open circuit subsonic wind tunnel was used. A two inch sandpaper strip was placed at the very front of the test section, spanning the width of the tunnel, in order to trip the flow to turbulent. The vortex generators were placed so that the trailing edge tips were 1.18 meters (m) downstream from the back of the sandpaper strip. The images were captured 3.175 millimeters (mm) from the trailing edge tips of the vortex generators. PIV data collection requires that the flow be seeded with particles that the camera can capture as the flow is illuminated by the pulses of the laser. The tunnel is seeded through a slit at the bottom of the wind tunnel. The tunnel was seeded for PIV with particles from a smoke machine using mineral oil. For plenoptic PIV, the seed particles need to be brighter and larger than the smoke used for the PIV. Therefore, silica beads were used and blown with fan mechanism into the slit on the bottom of the tunnel.

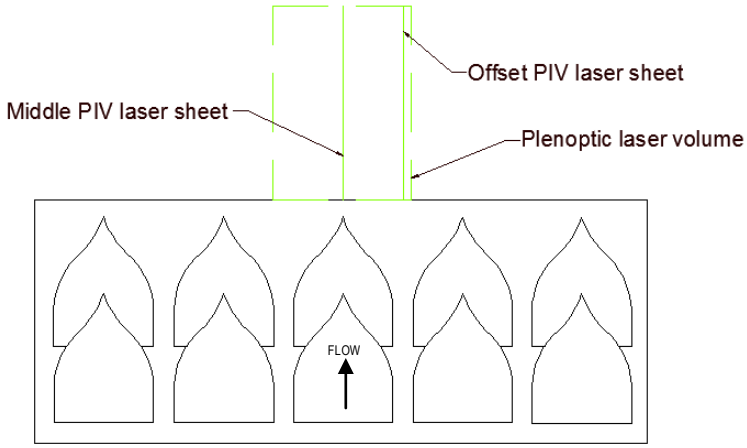

Figure 9. Laser sheets and volume locations (not to scale).

Three PIV runs were conducted. The first run was of flow over the wall with no VGs. Runs two and three used a VG array. The 2-D laser sheet was aligned directly at the center of the middle VG in the array for the second run. For the third run, the sheet was offset 22.2 mm. to the side of the tip of the center VG. These test frames were selected in order to see how the vortices shed from one VG interact with the neighboring vortices.

The plenoptic camera captures a volume rather than a sheet like the 2-D PIV. Therefore, only two runs were needed with the plenoptic camera since the flow aligned with the tip of the VG and the offset flow can be seen in the same volume. The first run was without VGs and the second run with the VG array. An experimental setup of the plenoptic PIV can be seen in Figure 10.

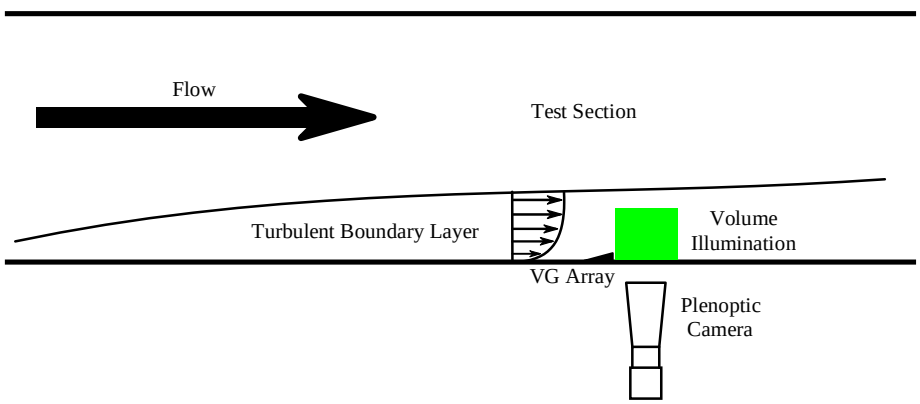

Figure 10. Plenoptic PIV experimental setup[13].

VI. Results

The flow is characterized though calculations from the PIV data gathered without any vortex generators. The freestream velocity was found to be 15.04 m/s and the boundary layer thickness, δ, was found to be 47.7 mm. The displacement thickness (δ^*) was calculated to be 4.41 mm. and the momentum thickness (θ) was 3.40 mm. These values result in a shape factor of 1.2965 which is within the normal turbulent flow range. Using momentum thickness as the length scale, the Reynolds number, Re_θ, was calculated at standard sea-level viscosity and density and found to be 4.20×10^4.

The boundary layer profile of the flow without any vortex generators is compared to the flow at the center of the VG array in Figure 11. A significant deformation in the profile can be seen at the middle of the VG array. There is a decrease in the velocity directly behind the VGs. This indicates that the flow goes through an adverse pressure gradient as it goes over the top of the vortex generators, decreasing the flow velocity. Adverse pressure gradients lead to flow separation, creating the wake behind the VGs described by Mokrani, et al. in Reference 3. When the data is collected at the location offset from the middle VG, the boundary layer profile deformation is less severe.

Instead, the boundary layer profile merely stretches, indicating an increase in the flow velocity near the wall. This demonstrates that the flow speeds up on either side of an individual VG in order to go around the VG. The fact that the deformation is slight also indicates that the effects of the VGs do not extend much outside the span of the VGs, nor does much interference between VGs seem to occur.

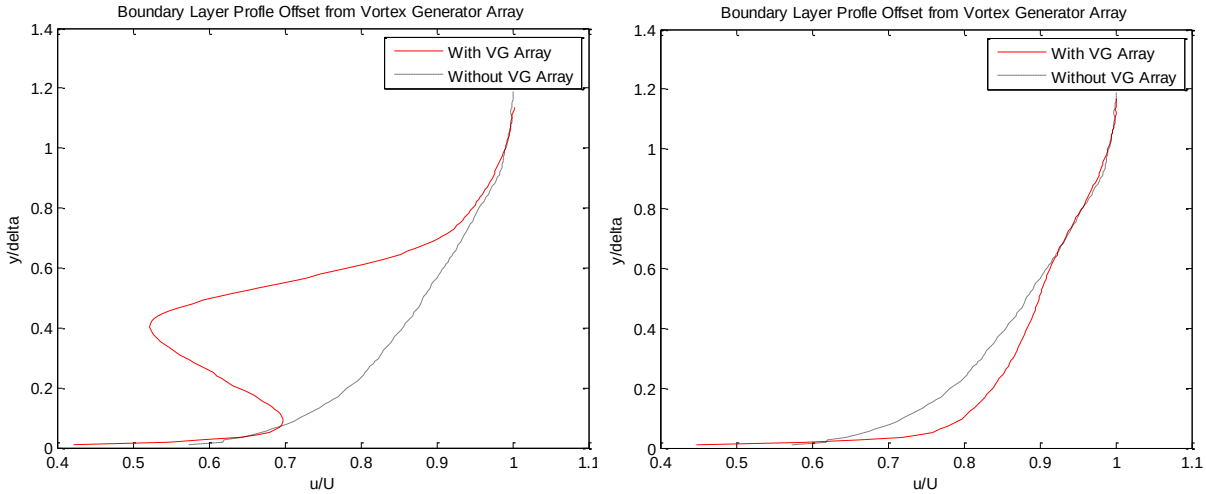

Figure 11. Boundary layer profile deformation with VGs

Due to time constraints and the preliminary nature of this work, only a single volume from the plenoptic camera is available. Seeding challenges also resulted in some unusable data since velocity vectors cannot be developed from images where the flow was under- or over-seeded. The plenoptic camera captures a complete 3-D vector field as shown in Figure 12 as a vector plot overlaid onto velocity iso-surfaces. The flow is moving from right to left. This volume is located just behind the vortex generators and extends downstream 38.1 mm., 38.1 mm. up from the bottom wall of the tunnel, and has a span-wise width of 57.15 mm. The volume is centered at the tip of the middle VG in the VG array.

Figure 12a shows the complete 3-D vector field volume behind the VG array. In Figure 12b, the stream-wise component of the velocity is shown by the iso-surface. The central blue area of the iso-surface indicates the wake that forms just behind the VGs, creating an area of low velocity. Above the low speed blue area, there is a section of higher velocity flow shown by the red, yellow, and orange area. This area represents the flow over the top of the VGs that must speed up, much as flow speeds up over the top of an airfoil. The high and low velocity areas centered behind the VG align with the observations of Mokrani, et al. in Reference 3. This high velocity flow above the low velocity wake creates the pressure gradient responsible for the counter-rotating trailing vortices characteristic of VG flow. The stream-wise velocity volume is also very consistent with the 2-D PIV data of this work, which is highly encouraging since the plenoptic camera is still a new and emerging technique. The consistency between the traditional PIV and the plenoptic PIV validates the use of plenoptic PIV for this flow field.

Figure 12c shows the iso-surface for the wall-normal component of the velocity. The green area close to the wall indicates wall-normal components of velocity that contribute to mixing between the inner and outer flow. However, the blue area indicates a return to the free-stream flow fairly rapidly away from the wall, as the wall-normal components of velocity drastically decrease to near zero values and the flow is almost entirely in the streamwise direction. In Figure 12d the span-wise component of the velocity is displayed by the iso-surface, indicating that for the majority of the flow, the span-wise velocity is non-zero and at magnitudes about half that of the freestream value of 15 m/s. This is a direct result of the vorticity produced by the VGs. Span-wise velocity is indicative of the counter-rotating trailing vortices and increased turbulence noted in almost all previous studies of vortex generators.

The plenoptic camera's uniqueness is that it can produce a full 3-D flow field. In order to compare the plenoptic results to conventional 2-D PIV results, 2-D slices can also be obtained. The PIV trials for the array of VGs were run with the laser sheet at two locations: one aligned with the middle VG, and one offset. Figure 13 shows the streamwise velocity vector components with an overlaid contour plot. Figure 13a shows a 2-D plenoptic PIV slice taken at the center of the volume and Figure 13b shows the traditional 2-D PIV image at the same area. Similarities between the images help to qualitatively validate the plenoptic camera. The wake behind the vortex generator can once again be seen in both images by the blue areas. The higher speed flow over the VGs can also be seen by the yellow and orange areas. Upward and downward velocity vectors at the divide between the wake and the high

velocity flow above it can be seen in both images. A significant downwash of the flow behind the VG, closing in the wake can also be seen by both shots.

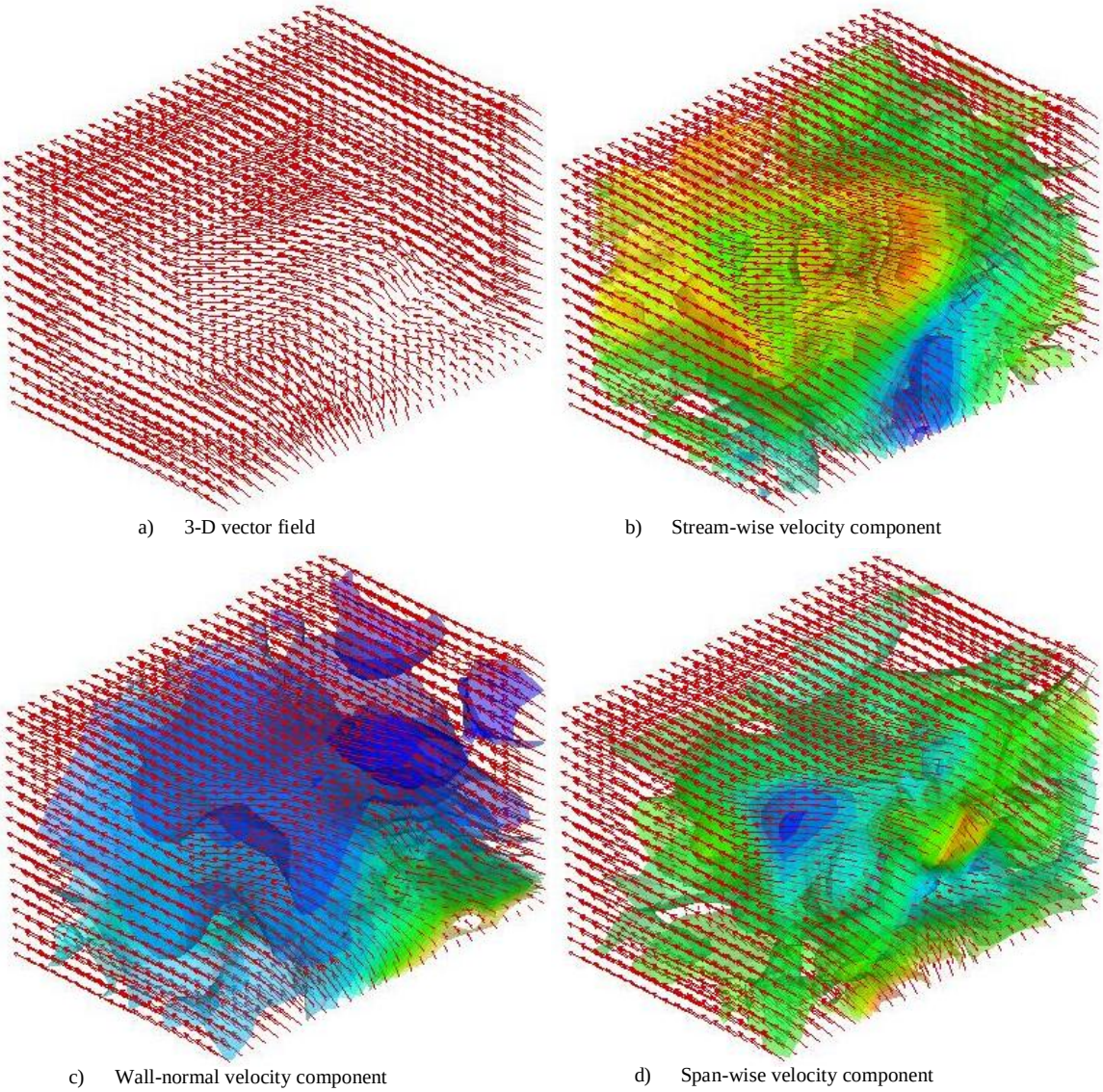

a) 3-D vector field

b) Stream-wise velocity component

c) Wall-normal velocity component

d) Span-wise velocity component

Figure 12. 3-D vector field and velocity iso-surface behind a VG array

Figure 13c shows a 2-D plenoptic PIV slice taken 6.35 mm. from the edge of the volume and Figure 13d shows the traditional 2-D PIV image offset at the same spanwise location. Both images also share the same flow features. Primarily, both show that the wake area is concentrated behind the vortex generators, but does not extend significantly span-wise between the generators. It can also be seen from both diagnostics methods that the stream-wise velocity field between VGs is a more constant, homogeneous field with velocities between around 10 m/s and 15 m/s (freestream value).

Differences between the two images are natural since they are of different instantaneous moments in the flow. However, they both show the same overall flow characteristics. Other differences can be attributed to the fact that the particle seeding varies between the two diagnostics methods. For the 2-D PIV, mineral oil through a smoke machine is used to seed the flow directly through a slit in the bottom of the tunnel. For the plenoptic PIV, a fan mechanism was used to seed the flow with silica beads through the slit in the bottom of the tunnel. The seeding methods for the plenoptic camera are still being fine-tuned since irregular seeding is possible for the plenoptic camera.

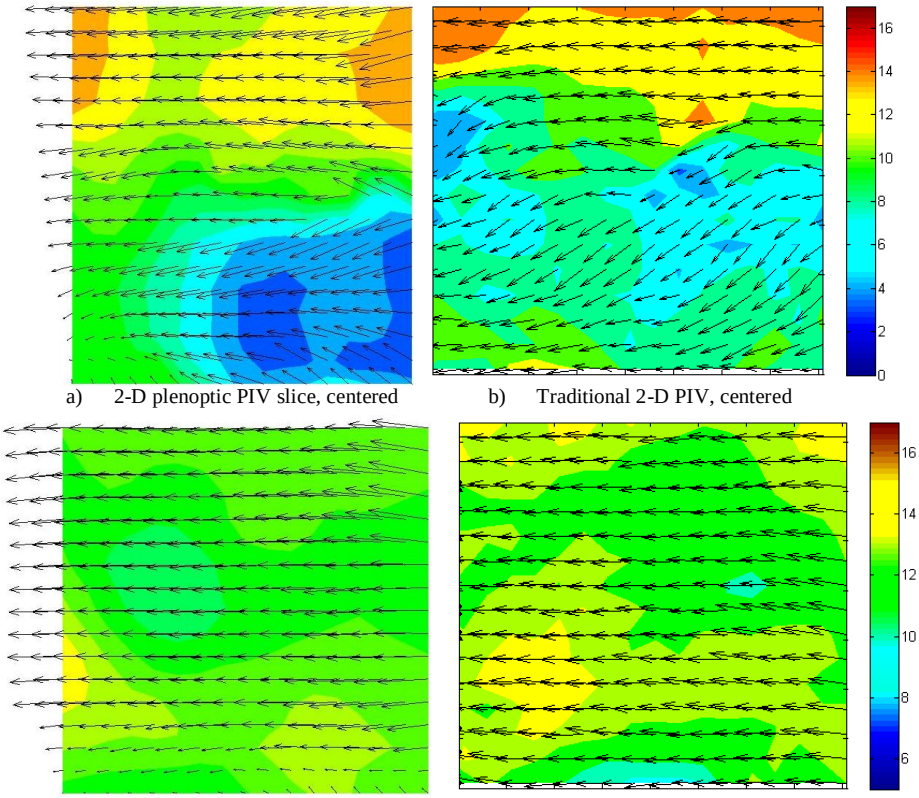

a) 2-D plenoptic PIV slice, centered b) Traditional 2-D PIV, centered

c) 2-D plenoptic PIV slice, offset d) Traditional 2-D PIV, offset

Figure 13. Traditional PIV compared to plenoptic PIV behind VG array

VII. Conclusion and Future Work

The 3-D characteristics of turbulent flow are crucial in understanding the nature of turbulent flow. In particular, the 3-D coherent structures that pervade turbulent boundary layers are of importance as they are critical in the relationship between the boundary layer and the outer flow. Current 3-D, 3-C techniques for studying flow are hindered by complicated optical setups and difficult post-processing procedures. The plenoptic camera uses digital light field imaging which records and saves as much data as possible for the given lens aperture. This storage of data allows for reconstruction and refocusing of the image to create a three-dimensional particle field. Therefore, it is logical and advantageous to combine light field imaging with the study of three-dimensional turbulent flow. The high potential of the plenoptic camera resides in the ease of setup combined with the ability to refocus the image.

The plenoptic camera has been shown to be a viable diagnostic method for studying vortex generators. The 3-D vector field captures similar flow characteristics to those observed in previous studies with VGs. The 2-D contour slices also compare well qualitatively to the traditional 2-D PIV images captured in this study. The primary differences between the 2-D contour slices and the 2-D PIV is thought to be due to the different flow seeding methods required for the two techniques. From one setup of the plenoptic camera, a full 3-D vector field is produced, allowing 3-D flow features to be studied. Traditional 2-D PIV type data can also be gathered in any plane, at any slice in the volume. The plenoptic camera offers more data from a single run than any other diagnostics method available.

This study of VGs with the plenoptic camera will continue in order to obtain more images at different areas in the flow. The issues with seeding the flow will also be addressed in order to develop a more consistent seeding method. Other immediate future plans include the use of the plenoptic camera to study other forms of passive flow control, such as different types of surface roughness. Three-dimensional irregular roughness will inherently produce three-dimensional effects in the boundary layer. The greatest influence of roughness on flow outside the boundary

layer is thought to be through the outer-length scale structures that penetrate the mean flow at the edges of the boundary layer. These structures are three-dimensional; therefore, the effect of surface roughness can best be studied using three-dimensional imaging and PIV techniques. Eventually, active flow control methods can also be studied with the plenoptic camera.

References

[1] Lin, Joehn C., "Review of research on low-profile vortex generators to control boundary-layer separation," *Progress in Aerospace Science,s* Vol. 38, 2002, pp 389-420.

[2] Koike, Masaru, Nagayoshi, Tsunehisa, and Hamamoto, Naoki, "Research on Aerodynamic Drag Reduction by Vortex Generators," *Mitsubishi Motors Technical Review,* Vol. 16, 2004, pp 659-671.

[3] Mokrani, A., Castelain, C., and Peerhossaini, H., "Experimental study of the influence of the rows of vortex generators on turbulence structure in a tube," *Chemical Engineering and Processing,* Vol. 48, 2009, pp 11-16.

[4] Lynch, Kyle P., and Thurow, Brian S., "Preliminary Development of a 3-D, 3-C PIV Technique using Light Field Imaging," *41st AIAA Fluid Dynamics Conference and Exhibit*.

[5] Thurow, Brian S., and Lynch, Kyle P., "Development of a High-Speed Three Dimensional Flow Visualization Technique," *AIAA Journal*, Vol. 47, No. 12, 2009, pp 2857-2865

[6] Anderson, John David. *Fundamentals of Aerodynamics*, 5th ed. New York: McGraw-Hill, 2011, Chaps. 1, 17.

[7] Davidson, P. A., *Turbulence: An Introduction for Scientists and Engineers*. Oxford, UK: Oxford University Press, 2004, pp. 4, 20-11, 18, 207-120, 118-119, 138-141.

[8] Kang, Yong-Duck, Choi, Kwing-So, and Chunz, Ho Hwan, "Direct Intervention of Hairpin Structures for Turbulent Boundary-layer Control," *Physics of Fluids,* Vol. 20, 2008, pp 20.

[9] Wu, Y. and Christensen, J.T., "Spatial Structure of a Turbulent Boundary Layer with Irregular Surface Roughness," *Journal of Fluid Mechanics,* Vol. 655, 2020, pp 380.

[10] Wheeler, Gary, "Means for maintaining attached flow of a flowing medium," Patent 4,445,045, 19 June 1984.

[11] Lu, Frank K.., Li, Qin, Shih, Yusi, Pierce, Adam J., and Lio, Chaoqun "Review of Micro Vortex Generators in High-Speed Flow," *49th AIAA Aerospace Sciences Meeting*.

[12] Ng, Ren, "Digital Light Field Photography," Ph.D. Dissertation, Computer Science Dept., Stanford University, Stanford, CA, 2006.

[13] Fahringer, Timothy W., and Thurow, Brian S., "Tomographic Reconstruction of a 3-D Flow Field Using a Plenoptic Camera," *42nd AIAA Fluid Dynamics Conference and Exhibit*.